

1

RESOURCE

2

3 **An ultra-fast, proteome-wide response to the plant hormone auxin**

4

5 Mark Roosjen^{1,*}, Andre Kuhn^{1,*}, Sumanth K. Mutte¹, Sjef Boeren¹, Pavel Krupar², Jasper
6 Koehorst³, Matyáš Fendrych², Jiří Friml^{4,#} and Dolf Weijers^{1,#}

7

8 1, Laboratory of Biochemistry, Wageningen University, Stippeneng 4, Wageningen, the
9 Netherlands

10 2, Department of Experimental Plant Biology, Charles University, Prague

11 3, Laboratory of Systems and Synthetic Biology, Wageningen University, Wageningen, the
12 Netherlands

13 4, Institute of Science and Technology Austria, Klosterneuburg, Austria

14

15 *, these authors contributed equally

16 #, corresponding authors: jiri.friml@ist.ac.at, dolf.weijers@wur.nl

17

18 Lead Contact: Further information and requests for resources and reagents should be directed
19 to and will be fulfilled by the lead contact, Dolf Weijers (dolf.weijers@wur.nl).

20

21

22

23

24 **SUMMARY (150 words)**

25

26 The plant signaling molecule auxin controls growth and development through a simple
27 nuclear pathway that regulates gene expresion. There are however several cellular and
28 physiological responses to auxin that occur within seconds, far too rapid to be mediated by
29 transcriptional changes, for which no molecular mechanism has yet been identified. Using a
30 phosphoproteomic strategy in *Arabidopsis thaliana* roots, we identify an ultra-rapid auxin
31 response system that targets over 1700 proteins, many within 30 seconds. Auxin response is
32 chemically specific, requires known auxin-binding proteins, and targets various pathways.
33 Through exploring its temporal dynamics, we infer auxin-triggered kinase-substrate networks
34 and identify apoplastic pH changes as a target of signaling and as part of a relay mechanism.
35 By generating a variety of phosphoproteomic datasets, integrated with structural information
36 in a web-app, and by demonstrating analysis and inference strategies, we offer a resource to
37 explore rapid and dynamic signaling in plants.

38

39

40 **KEYWORDS**

41

42 Auxin, signaling, protein phosphorylation, kinase networks, apoplastic pH

43

44

45

46 **INTRODUCTION**

47

48 Since its discovery nearly a century ago^{1,2}, the plant signaling molecule auxin has been the
49 focus of intensive investigation³. The naturally occurring indole 3-acetic acid (IAA) is
50 widespread in nature and found in essentially all plants studied to date⁴. Its biological activity
51 as a signaling molecule, acting at nanomolar to micromolar concentrations, is extremely
52 profound. When applied to plants or plant cells, auxin can trigger a wide range of
53 physiological, cellular and molecular changes that likely underly the long-term effects on
54 plant growth and development. Classical examples of auxin activity include mediating tropic
55 growth (e.g. phototropism or gravitropism)^{1,2,5,6}, as well as the promotion of vascular cell
56 differentiation⁷⁻⁹, and the induction of adventitious or lateral roots^{10,11}. Molecular and cellular
57 responses to auxin include rapid changes in membrane chemical potential, associated changes
58 in ion transport¹²⁻¹⁵, changes in the velocity of cytoplasmic streaming^{16,17}, changes in cellular
59 growth rate and differentiation^{11,18-20}, and importantly, reprogramming of transcription²¹.

60 To identify the mechanisms underlying the responses to auxin that control plant
61 growth, genetic screens have led to the isolation of a range of *Arabidopsis* mutants that are
62 insensitive to auxin's growth-inhibiting action²²⁻²⁴. Cloning of the affected genes, followed
63 by detailed molecular, biochemical and structural analysis have revealed a simple, yet
64 powerful mechanism for auxin response²⁴. In what is referred to as the Nuclear Auxin
65 Pathway (NAP), auxin enables interaction of Aux/IAA transcriptional inhibitors with a
66 ubiquitin ligase complex (SCF^{TIR1/AFB}) to promote their degradation. This liberates DNA-
67 binding ARF transcription factors from Aux/IAA inhibition and allows transcriptional control
68 of their many target genes (reviewed in²¹). This NAP can account for many of the observed
69 auxin activities across land plants and in many developmental contexts, including responses
70 to environmental signals³. However, the time required to bring about changes in cellular
71 physiology through transcriptional control is substantial, and limited by the velocity of
72 transcription, translation, protein folding and targeting. Hence, even if the first IAA-induced
73 transcripts are visible between 5-10 minutes after IAA treatment²⁵, it is extremely unlikely
74 that the NAP can account for the changes in e.g. ion fluxes, cellular growth and subcellular
75 traffic that have been observed to occur within seconds to minutes^{12,14,16,17,26,27}. It is therefore
76 inevitable that there exists a second auxin response system that is kinetically suited to
77 mediate such rapid responses. Indeed, several "non-canonical" auxin responses have been
78 reported^{14,26,28} that do not rely on a (complete) NAP, but that may involve one of its
79 components. For example, fast inhibition of *Arabidopsis* root growth and changes in

80 membrane polarity involve the AFB1 receptor of the NAP¹⁴. Other rapid responses including
81 the activation of H⁺-ATPases at the plasma membrane for growth regulation^{27,29} and
82 cytoplasmic streaming, possibly related functions in endocytic trafficking^{16,30} require a cell
83 surface auxin signaling mediated by the ABP1 auxin receptor and its associated TMK
84 receptor-like kinase³. Thus, the existence of fast responses to auxin is evident, but it is
85 unclear what mechanisms and response system(s) might underlie such fast responses.

86 Here, we explore the role that reversible protein phosphorylation may play in fast
87 responses to auxin. Protein phosphorylation is a widespread mechanism for enzymatically
88 modifying the structure and function of pre-existing proteins³¹, thus eliminating the need for
89 *de novo* protein synthesis. Given that phosphorylation depends only on the (allosteric)
90 activation of a protein kinase, the reaction is intrinsically rapid. Several well-known examples
91 of phosphorylation-based signaling exist across the kingdoms of life³²⁻³⁵. Among these, some
92 are particularly rapid, with Insulin and EGF ligands triggering initial phosphorylation
93 changes by receptor kinases within seconds^{34,35}, followed by relays and amplification steps
94 with additional protein kinases³⁵. Phosphorylation-based signaling is also widespread in
95 plants, and mediates responses to peptide ligands in development and immunity³³, as well as
96 to Brassinosteroids³⁶⁻³⁸. Whether phosphorylation-based signaling is a meaningful
97 component in auxin response is an open question. There is ample evidence for
98 phosphorylation-based events in the control of activity and localization of PIN auxin
99 transporters³⁹. Whether however, these events are part of a rapid signaling system is an open
100 question. The TMK1 receptor-like kinase mediates IAA-triggered phosphorylation changes,
101 even within two minutes^{16,27}, but the scope or dynamics of this response is unclear, given that
102 the number of targets reported is limited.

103 Here, we used a phosphoproteomics strategy to address if a fast response system to
104 IAA built on protein phosphorylation, exists. Prior phosphoproteomic analysis of auxin
105 response has been reported in both *Arabidopsis*^{27,40,41} and rice⁴². In rice, a 3-hour treatment
106 was reported⁴², while in *Arabidopsis*, treatments used the synthetic auxin analogue 1-NAA
107 for either 2 hours⁴⁰ or 11 days⁴¹, leaving the question of whether naturally occurring auxin
108 can trigger phosphorylation changes at the same scale. We recently reported that IAA can
109 trigger changes in protein phosphorylation in *Arabidopsis* roots within 2 minutes and that this
110 response requires ABP1 and TMK1²⁷. However, it is entirely unclear what the specificity,
111 kinetics, scope and targets of this response are.

112 Here, we show that auxin triggers changes in the phosphorylation of hundreds of
113 proteins in *Arabidopsis* roots well within 30 seconds. An extended time series showed that

114 over two thousand proteins are differentially phosphorylated within 10 minutes, with a range
115 of temporal dynamics. Analysis of mutants suggests these responses to involve both
116 intracellular and extracellular auxin perception. We leveraged the rich datasets to identify
117 pathways and functions that are triggered by rapid auxin signaling, predict signaling hub
118 kinases and demonstrate a very rapid effect on apoplastic pH. Lastly, we compiled the
119 datasets in a searchable web tool, integrated with protein structural information. We thus
120 identified a novel layer in auxin response with profound impact on many cellular pathways
121 and functions, and created a resource that will form the starting point for renewed
122 mechanistic investigation in the underexplored area of fast auxin response.

123

124 **RESULTS**

125

126 **Identification of a specific, rapid, phosphorylation-based auxin response**

127

128 To explore the ability of *Arabidopsis* roots to respond to auxin by changing protein
129 phosphorylation levels, we initially treated roots with a concentration (100 nM) of the
130 naturally occurring auxin Indole 3-Acetic Acid (IAA) that is sub-maximal with regards to
131 physiological responses. The earliest recorded transcriptional responses to auxin treatment
132 occur after 5-10 minutes^{25,43}. Also given theoretical considerations related to gene expression
133 and protein synthesis, we chose a 2 minute treatment time for mapping phosphorylation
134 changes, assuming that any changes seen at that time are not influenced by changes in
135 transcription. Using statistical analysis across 4 biological replicates, we next identified
136 differential phosphosites (note that these are mapped to protein groups – not necessarily
137 individual proteins, if there are multiple close homologs). We optimized the treatment and
138 sample preparation procedure and measured samples on multiple mass spectrometers, and
139 found the results to be very robust. Two minutes IAA treatment on *Arabidopsis* roots
140 changed the abundance of 1048 phosphosites (FDR ≤ 0.01), where 666 were more and 382
141 were less abundant after IAA treatment (Figure 1A). We performed shotgun proteomic MS
142 measurement on equivalent samples (Figure 1B), which suggest that observed changes in
143 phosphosite abundance are not generally caused by altered protein levels. Likewise, the
144 differentially phosphorylated proteins showed little overlap with transcriptionally regulated
145 genes (Figure S1A). We therefore regard these changes as hyper-/hypo-phosphorylation
146 events.

147 The vast effect of a 2-minute IAA treatment on the phosphoproteome to this low IAA
148 concentration is striking, and suggest this to be a hormonal response. However, auxin is a
149 weak organic acid derived from Tryptophan, and it is possible that (part of) the response
150 observed is an unspecific response to weak organic acids or auxin-like molecules. To test
151 chemical specificity, we therefore used a panel of related chemicals (all at 100 nM) in the
152 same set-up, and measured phosphoproteomes after 2 minutes treatment. None of the
153 synthetic auxin analogs 2,4-Dichlorophenoxy-acetic acid (2,4D), 1-Naphthaleneacetic Acid (1-
154 NAA) or 2-Naphthaleneacetic Acid (2-NAA) trigger phosphorylation changes that showed any
155 correlation to those induced by IAA (Figure 1C; Spearman's rank correlation [R]: 0.12 for
156 2,4-D; 0.07 for 1-NAA and 0.01 for 2-NAA). Likewise, neither Benzoic Acid (BA; R=0.25)
157 nor Formic Acid (FA; R=0.20) induced IAA-like phosphorylation changes (Figure 1C). As a

158 control, two entirely independent IAA treatments and measurements (Figure 1D) showed
159 strong correlation ($R=0.77$). Thus, IAA response is chemically specific. Synthetic auxins
160 have auxinic activity in several physiological assays, and it is therefore striking that 2,4-D, 1-
161 NAA and 2-NAA failed to trigger IAA-like phosphorylation changes. To test if these can act
162 like IAA in this response, albeit less efficiently, we measured phosphoproteomes at a 10-fold
163 higher concentration (1 μ M). Indeed, at this concentration, 1-NAA ($R=0.90$) and 2-NAA
164 ($R=0.88$) could induce IAA-like phosphorylation changes, but BA could not ($R=0.12$; Figure
165 S1B). Thus, IAA induces a rapid, chemically specific, hormonal phosphorylation response in
166 Arabidopsis roots.

167

168 **Auxin phospho-response is ultra-rapid and dynamic**

169

170 To explore the temporal dynamics of the newly identified phosphorylation response, we
171 generated a time series of IAA treatments on Arabidopsis roots, ranging from 30 seconds to
172 10 minutes. To ensure that this time series was not confounded by auxin-independent effects
173 of submerging roots in growth medium, we also sampled solvent mock controls for each time
174 point, and subtracted the phosphosite abundance in the mock treatment from each IAA
175 treatment (Figure 2A). This led to a set of unique phosphoproteomes that could be clearly
176 resolved by Principal Component Analysis (PCA; Figure 2B). Strikingly, even at 30 seconds,
177 IAA triggered changes in abundance of hundreds of phosphosites (Figure 2D), underlining
178 the rapid nature of the response. Compiling all differentially phosphorylated sites across the
179 entire time series, a total of 2962 phosphosites is regulated by IAA (Figure 2D),
180 corresponding to 1770 proteins, representing ~5% of the proteins encoded by the Arabidopsis
181 genome.

182 We next used the Minardo-Model⁴⁴ to order groups of phosphopeptides that show
183 similar trends of phosphorylation (Figure 2D). In each cluster, generalized linear models are
184 derived from individual profiles which, together with Z-scores and post hoc Tukey test, infers
185 event windows at which the majority of profiles show half-maximal amplitude response.
186 From this analysis, the earliest events likely occur well within 30 seconds after treatment
187 (Figure 2D; Clusters 1-9). This analysis clearly identified a range of temporal patterns in
188 IAA-dependent phosphorylation. These ranged from transient, early or late hyper- or hypo-
189 phosphorylation to gradual hyper- or hypo-phosphorylation, and oscillatory hyper- and hypo-
190 phosphorylation (Figure 2D).

191 Phosphorylation events are often counteracted by regulatory dephosphorylation in
192 enzymatic feedback loops. Given the highly dynamic phosphorylation patterns upon IAA
193 treatment, it is possible that such feedbacks are operating here. To test the reversibility of the
194 widespread IAA-induced differential phosphorylation, we performed a 2-minute IAA
195 treatment, followed by 5-minute washout treatment with IAA-less medium. If the response
196 were reversible, the profile after washout should resemble that after 2 minutes, or even before
197 IAA treatment. Instead, PCA analysis of the washout treatment, along with the time series,
198 grouped the washout treatment with the 10-minute treatment (Figure 2B). This suggests that
199 the IAA response is not globally reversible and persists for minutes even after removal of the
200 signal.

201

202 **Genetic requirements of rapid auxin response**

203

204 The widespread phosphorylation response to IAA treatment is novel, and a key question
205 therefore is what mechanism mediates it. We initially explored the likely location of the
206 receptor or binding site for IAA. As a weak acid, IAA tends to be protonated in the apoplast,
207 and can enter the cell to some degree. Import into the cytosol is however facilitated by the
208 AUX1 permease⁴⁵. To ask if the binding site for IAA is intracellular or apoplastic, we
209 measured a time series phosphoproteome in the *aux1-100* mutant (Figure 2C). In case auxin
210 is perceived intracellularly, one would expect a delay in the response. The *aux1* mutant did
211 show a substantially different phosphorylation pattern, and PCA analysis showed clear
212 separation of wild-type and mutant, irrespective of IAA treatment (Figure 2C). Importantly
213 however, the *aux1* mutant showed a profound response to IAA, even at 30 seconds, which
214 suggests that facilitated IAA influx is not strictly required for fast response. Hence, at least
215 some of the IAA binding capacity for this fast response likely resides in the apoplast.

216

217 Two auxin binding sites have been studied in detail: the nuclear TIR1/AFB receptors
218 mediate auxin-dependent gene regulation, as well as some rapid non-transcriptional
219 responses^{14,26,28}. For the latter, the cytosolic AFB1 protein appears to play a prominent role¹⁴.
220 The ABP1 protein resides both in the endoplasmic reticulum and in the apoplast, and has
221 been connected to non-transcriptional responses, likely through interactions with the TMK1
222 receptor-like kinase¹⁶. We compared previously recorded¹⁶ phosphoproteomes in *abp1* and
223 *tmk1* mutants with one generated of the *afb1* mutants after a 2-minute IAA treatment.

224

225 Strikingly, each of the three mutants showed profound changes in their auxin-induced
226 phosphoproteomes (Figure 3A,C). In all three mutants, a significant fraction of the auxin-

225 triggered changes in phosphorylation were lost, or in cases, oppositely regulated (Figure 3A).
226 To address that effect of each mutation on the level of phosphorylation of IAA-regulated sites
227 in the absence of external IAA treatment, we compared mock-treated mutants with wild-type
228 and evaluated the phosphorylation level of the entire set of IAA-triggered differential sites.
229 This analysis showed that IAA-induced phosphosites are strongly hypophosphorylated in
230 untreated *abp1* and *tmk1* mutants, but not in *afb1* (Figure 3B). Thus, *abp1* and *tmk1*
231 accumulate phosphorylation defects during their normal growth, while this is not the case for
232 *afb1*. Quantitatively, the number of IAA-triggered differential phosphosites was strongly
233 reduced in all three mutants (Figure 3D). When clustering mutants according to the similarity
234 of the changes in phosphorylation levels across the entire set of IAA-dependent
235 phosphopeptides (in wild-type), we found that *abp1* and *tmk1* clustered together, and *afb1*
236 showed a distinct effect on the global IAA-triggered phosphoproteome (Figure 3E).
237 Strikingly, a large set of phosphosites was similarly affected in *abp1* and *tmk1* mutants, and
238 oppositely affected in the *afb1* mutant (Figure 3E). This behavior is clearly illustrated by
239 examples of individual phosphosites a range of proteins (Figure 3F). This demonstrates that
240 ABP1, TMK1 and AFB1 are all required for normal auxin-triggered phosphorylation, and
241 that ABP1 and TMK1 act coordinately, while AFB1 generally opposes ABP1/TMK1 action.

242

243 **Auxin-dependent phosphorylation targets multiple cellular pathways**

244

245 To explore the range of cellular functions potentially targeted by IAA through
246 phosphorylation, we initially mined the full set of differential phosphosites for
247 overrepresented functions, families and pathways. Gene Ontology (GO) analysis of
248 differential phosphosites (Figure 4A) showed that a broad range of cellular functions is
249 subject to regulation. These include a plethora of processes at the plasma membrane or
250 endomembranes, such as endocytosis, vesicle fusion and ion transport, but also prominently
251 featured nuclear processes such as transcription, chromatin structure and splicing. While
252 there is very strong enrichment of plasma membrane, cytosolic and nuclear proteins, most
253 cellular locations are targeted by auxin-triggered phosphorylation. Based on this GO analysis,
254 the prediction is that many aspects of cell function are targeted by IAA-triggered
255 phosphoregulation.

256

257 We next surveyed the dynamic phosphorylation of proteins within functional groups
258 that had been linked to auxin action, phosphorylation or were clearly enriched in the GO
analysis (Figure 4B). PIN phosphorylation is a well-known regulatory step in transporter

259 activation or polar localization. We identified a range of phosphosites on PIN1, 2, 3 and 7.
260 While most were rapidly hyperphosphorylated, those on PIN1 were hypophosphorylated.
261 Interestingly, these all represent sites that have not previously been connected to PIN
262 regulation. We likewise found rapid hyperphosphorylation on the ABCB19 auxin transport
263 protein.

264 Auxin profoundly regulates gene expression, a function that has thus far been
265 connected to the NAP system²¹. We noticed that there is a very rapid hypophosphorylation on
266 a range of proteins involved in chromatin structure and activity. This includes BRM and SYD
267 SWI/SNF ATPases and nearly all members of the TPL/TPR family. The function of these
268 events is not known, but there it is likely that early phosphorylation events prime or condition
269 later transcriptional responses.

270 A third functional group that is strongly affected by auxin is cell wall and cytoskeletal
271 proteins. We found many differential phosphosites on Cellulose Synthases, Microtubule
272 Associated Proteins, Myosins, and Dynamin Related Proteins. There was no clear pattern in
273 hyper/hypo-phosphorylation among these, and in some cases, the same protein was
274 oppositely affected at different residues.

275 Lastly, IAA appears to trigger a range of phosphorylation events in mediators of
276 signaling for other plant hormones. For example, multiple proteins in the ethylene pathway
277 (ACS8, CTR1, EIN2) are targeted, as are multiple brassinosteroid (BES1, BZR1, BSL2,
278 BSK2) and ABA (ABF4, PYL1), and the jasmonic acid component MYC2. Thus, while most
279 of these sites are not yet connected to activity of these factors, it is evident that rapid IAA
280 signaling has the potential to influence the response to other plant hormones.

281 The phosphorylation changes reported here offer a rich source of data that allows
282 developing hypotheses for future studies. To facilitate the use of this rich dataset and to help
283 interact with the data, we designed a webtool (AuxPhos;
284 <https://weijerslab.shinyapps.io/AuxPhos>) and user interface. AuxPhos allows to search
285 individual proteins by their unique identifier, and visualize the quantification of its
286 phosphopeptides across the various datasets (wild-type with IAA and various related
287 chemicals; time series; *aux1*, *abp1*, *tmk1* and *afb1* mutants). In addition to offering a
288 searchable interface for navigating phosphoproteins, we have implemented AlphaFold2-
289 based protein structural models to visualize on predicted protein structures, where differential
290 phosphorylation occurs. An examples of such visualizations on the EIR1/PIN2 protein are
291 shown in (Figure 4C). As further phosphoproteomic data will become available, these will be
292 integrated in the tool.

293

294 **Identification of kinases in auxin-triggered phosphoresponse**

295

296 Given the availability of a densely sampled time series and the identification of nearly 3000
297 phosphosites, we asked if the dataset could be used to infer phosphorylation relationships. To
298 this end, we filtered the entire phosphoproteome dataset for phosphosites in the (predicted⁶⁷)
299 activation loop of the full set of *Arabidopsis* kinases (Figure 5A). This identified 26 kinases
300 that were differentially phosphorylated in their activation loop during the IAA-triggered time
301 series (Figure 5B), most of which were hyperphosphorylated, likely signifying activation of
302 kinase activity. We next performed a regression analysis (Figure 5A) where we identified
303 phosphorylation sites that temporally matched or followed the dynamics of activation of each
304 kinase, obeying several statistical criteria. This led to the generation of a kinase-target
305 network encompassing all 23 regulated kinases and 2140 phosphotargets (Figure S3). To test
306 the validity of this inference approach, we asked if protein kinases with known
307 phosphotargets were correctly predicted. This analysis is challenging because of the relatively
308 small number of well-documented kinase-substrate relationships with information about the
309 exact phosphosite. Nonetheless, we found several such pairs to conform to their predicted
310 relationship in our dataset: A RAF kinase was connected to its OST1 target, and this OST1
311 kinase to a bZIP target. In addition, D6PK was connected to PIN7 (Figure 5C), consistent
312 with PIN phosphorylation by this kinase⁴⁶.

313 We next ranked the 23 kinases according to their weight and position in the
314 phosphonetwork (Figure 5D), indicated by their degree and their betweenness centrality.
315 These two parameters were correlated in this network. This identified several kinases as
316 potential hubs in this network. These include the D6PK kinase, as well as the LRR-RLK
317 protein LRR1, a group of closely related RAF kinases and PIP5K2. The latter is a
318 phosphoinositide kinase, and it is an open question if the PIP5K activity or the membrane
319 changes it induces are correlated with downstream phosphorylation. In any event, this
320 network analysis offers a prioritized set of auxin-regulated kinases that are strong candidates
321 for mediating rapid responses.

322

323 **Rapid auxin response controls membrane polarization**

324

325 The many functions enriched in the IAA-dependent phosphoproteome include the control of
326 intracellular pH (Figure 4A), which we explored further given that membrane polarity and

327 apoplastic pH have been shown to be subject to auxin control^{14,15,27,29,47}. To explore this
328 regulation in more detail, we analyzed phosphorylation dynamics of the family of
329 Arabidopsis H⁺-ATPase (AHA) proton pumps. These directly transport protons across
330 membranes and tend to be localized to the plasma membrane, thus directly controlling
331 apoplastic pH and membrane polarity^{14,27,29}. One AHA is directly phosphorylated by
332 TMK1^{27,29}, and we indeed found both TMK1 and AHA1/2 phosphorylation to be rapidly
333 induced (Figure 6A). Likewise, most AHA proteins are differentially phosphorylated within
334 30 seconds, followed by protein-specific temporal dynamics. This suggests a family-wide
335 regulation of AHA pumps, and predicts that IAA treatment triggers profound and very rapid
336 apoplastic pH changes. Previous pH imaging showed that IAA acts on apoplastic pH within
337 minutes²⁷, but did not allow to dissect early kinetics. We therefore used the pH-sensitive
338 HPTS dye⁴⁷ to measure root surface pH changes in a line expressing the cytosolic calcium
339 sensor R-GECO1⁴⁸. We imaged roots in a microfluidic device mounted on a vertical
340 microscope to record the apoplastic pH response in the seconds immediately following auxin
341 application. We found that IAA treatment led to an almost instantaneous apoplastic
342 alkalinization, represented by an increase in HPTS fluorescence excited by 488 nm laser
343 (Figure 6B). After reaching a peak at 90 seconds, the surface pH decreased to a new plateau
344 which was more alkaline than the pre-treatment levels. This behavior is consistent with the
345 hypothesis that auxin causes a proton influx into cells, which is counteracted by the activation
346 of proton extrusion from the cells²⁷, and this two-phase process is reflected in the dynamics
347 of AHA phosphorylation. Their complex phosphorylation pattern likely results from a direct
348 activation by the TMKs as well as indirect activation by auxin-induced ion fluxes.

349 The finding that IAA treatment triggers very rapid pH changes, raises the possibility
350 that the pH changes are themselves causal to some of the later phosphorylation events
351 observed after IAA treatment. To address this question, we treated seedlings with the fungal
352 toxin Fusicoccin (FC), a compound that causes continuous activation of H⁺-ATPases^{50,52}, and
353 recorded phosphoproteomes on dissected roots. A 5-minute FC treatment indeed induced
354 differential phosphorylation on 1097 proteins (Figure 6C). When comparing these
355 phosphosites to those triggered by IAA, we found that more than of half the FC-induced
356 changes are also triggered by IAA, and about 20% of the IAA-induced changes are also
357 triggered by FC (Figure 6D). This suggests that IAA triggers a unique and specific early set
358 of phosphorylation changes, that includes regulatory changes to the H⁺-ATPases. The
359 changes in pH that ensue from this ATPase regulation then themselves in part trigger a
360 second wave of phosphorylation changes. The FC & IAA-triggered phosphosites include the

361 AHA proteins themselves, suggesting feedback regulation (Figure 6E), but also include PIN
362 and ABCB auxin transporters and ACA Calcium ATPases. Accordingly, IAA treatment also
363 led to near instantaneous calcium influx, which reached a peak after 60 seconds and then
364 reverted to a new plateau (Figure 6F, Supplemental Figure 4), which, similarly to the surface
365 pH, was higher than the pre-treatment level. This is consistent with the tight connection
366 between the regulation of pH and calcium signaling in plant cells⁴⁹. In conclusion, IAA
367 triggers a highly dynamic, and likely feedback-regulated set of changes in membrane ion
368 fluxes and the dynamics of these events is well reflected in the phosphoproteome dataset.

369

370 DISCUSSION

371

372 Through phosphoproteomic profiling, we have identified a previously unknown and
373 unsuspected branch of auxin activity. Strikingly, *Arabidopsis* root cells are capable of
374 changing the phosphorylation state of more than 1700 proteins within 10 minutes of
375 treatment with the natural auxin IAA, many of which respond within 30 seconds. We have
376 not explored yet earlier timepoints, as these become technically impractical to harvest and
377 perhaps effectivity will also be limited by the speed of IAA diffusion into roots.
378 Computational inference suggests that the earliest responses occur around 20 seconds, a
379 timeframe that is consistent with the kinetics of insulin-triggered phosphorylation in animal
380 cells³⁵. This auxin-triggered phosphorylation response is remarkably chemically specific,
381 with natural IAA being substantially more effective than synthetic analogs, and related – but
382 physiologically inactive – compounds being unable to trigger the response. This suggests a
383 specific auxin binding site for this response. We explored the role of the cytoplasmic and
384 nuclear AFB1 receptor, as well as the extracellular ABP1 protein, along with its interaction
385 partner TMK1. These analyses show that matters are not simple: all three proteins are
386 required for IAA-dependent phosphorylation, but in different ways. Globally, the *afb1*
387 mutation has essentially opposite effects to either *abp1* or *tmk1* mutants, which are highly
388 similar¹⁶. Genetically speaking, these could therefore be interpreted as antagonistic
389 components converging on a shared downstream process. At what level these intersect is a
390 question for future investigation, but it is striking that also with regards to controlling
391 apoplastic pH, the nuclear auxin response and TMK1-dependent response have opposite
392 activities²⁷.

393 One caveat of the analysis is that it relies on adding exogenous IAA for observing
394 changes in phosphorylation. One could argue that these treatments do not reflect regulatory

395 events that occur in the absence of external auxin. However, even untreated *abp1* and *tmk1*
396 mutants show hypophosphorylation of many of the sites that are hyperphosphorylated upon
397 IAA treatment in wild-type. This suggests that this same set of sites is controlled by these
398 proteins under normal growth conditions, likely by endogenous IAA, and that defects in their
399 phosphorylation accumulate over time in mutants. The further identification of components in
400 auxin-triggered phosphorylation will likely help to connect these regulatory events to cellular
401 physiology.

402 The scope of this auxin response is vast, and targets a multitude of proteins, pathways,
403 organelles and functions. Several known or suspected auxin-related proteins are among these,
404 for example PIN and ABCB auxin transporters. Identifying these sites now allows the
405 formulation of specific hypothesis regarding their regulatory role. As a proof of concept in
406 using this resource, we have explored the proton and Calcium fluxes across the plasma
407 membrane that are predicted by the phosphoproteome data. In addition to validating such
408 predictions, we also demonstrate a causal role of apoplastic pH changes in triggering further
409 phosphorylation changes.

410 A key question is what the impact of this response is on cellular physiology, structure,
411 growth and development. From the many pathways affected, one could expect disruption of
412 the response to have strong phenotypic consequences. It is therefore surprising that the three
413 mutants that strongly affect this response (*abp1*, *tmk1* and *afb1*) all have largely normal
414 development^{16,51,53,54}. Each of these mutants has phenotypic defects in germination (*afb1*)⁵¹,
415 regeneration (*abp1* and *tmk1*)¹⁶ or cytoplasmic streaming (*abp1* and *tmk1*)¹⁶. However, these
416 are subtle. One interpretation is that the phosphorylation network is highly non-linear, with
417 multiple sites being targeted on proteins, phosphatases counteracting kinases, and complex
418 functional redundancies. Given the speed of phosphorylation, it is well possible that the ease
419 of perturbation is balanced by biochemical robustness. It will be interesting to discover the
420 key hubs in the phosphorylation network to understand both the physiological function and
421 the mechanisms underlying robustness. It should be added that this set of mutants has been
422 studied mostly, if not exclusively, under lab-grown, controlled conditions. It is possible that
423 this response system mediates a function that is required in the ecologically relevant setting,
424 and less so in well-controlled conditions.

425 In relating the phosphorylation response to biology, an important consideration is
426 where this response occurs. We have sampled only roots, for purposes of reproducibility and
427 limiting tissue complexity. It does raise the question of whether similar changes occur – and
428 pathways are affected – in other plant parts. Limitations to sensitivity of mass spectrometry

429 currently make it essentially impossible to capture phosphoproteomes of root cell types, even
430 if just because such analysis require tissue dissociation which would preclude studying rapid
431 responses. When examining the proteins targeted, many are expressed beyond roots, and it
432 would appear reasonable to assume that a response as profound as this is not limited to a
433 single cell type or organ.

434 When exploring the proteins and functions targeted by IAA-triggered
435 phosphorylation, several stand out. Firstly, mediators of other hormone pathways are
436 prominently regulated. One interesting example is the EIN2 protein^{55,56}. This protein is
437 known to be phosphorylated by the CTR1 kinase on two Serines (645 and 924) to control
438 nuclear localization in response to ethylene^{55,56}. Both these sites are hypophosphorylated
439 rapidly following IAA treatment, which predicts that IAA rapidly alters EIN2 localization
440 and ethylene response. Another interesting case is the coordinated hypophosphorylation of a
441 slew of chromatin regulators. This includes BRM and SYD SWI/SNF ATPases and TPL/TPR
442 co-repressors that are all involved in mediating IAA-regulated transcriptional responses⁵⁷⁻⁵⁹.
443 The functional impact of these phosphorylations – if any – is unknown. However, it is very
444 likely that the rapid response system interacts with subsequent transcriptional responses,
445 perhaps by priming cells for gene regulation upon prolonged exposure. In any case, our
446 findings reveal the tremendous molecular changes occurring in cells treated with auxin in the
447 minutes prior to the time window during which transcriptional activity is normally recorded.

448 Lastly, we would like to emphasize the strength of combining ultra-rapid, dense and
449 successive sampling in this approach. We are not aware of other studies using a similar
450 approach to infer the dynamics of any form of rapid signaling in plants. Here, we have
451 leveraged the data to predict kinase-substrate relationships based on regression of temporal
452 profiles. These are successful in capturing known relationships, and help to predict a set of
453 strong candidate kinases that may mediate aspects of auxin-triggered rapid signaling, and will
454 be subject of future investigation. In the accompanying paper (Kuhn, Roosjen et al.,
455 accompanying manuscript), we report the identification of a key mediator of rapid phospho-
456 signaling in part through this inference strategy. We expect that similar strategies as reported
457 here will be instrumental in resolving causalities and identifying regulators in responses to
458 other signals, whether hormones, endogenous peptides or environmental or microbial signals.

459 With reporting this novel, unsuspected and vast response, we offer a new avenue in
460 studying a profoundly important plant signaling molecule. Not only is auxin a major regulator
461 of “normal” plant growth and development, it is also a potent herbicide and growth regulator
462 in agricultural and horticultural practice. We anticipate that mining the rich datasets,

463 compiled in the AuxPhos tool (<https://weijerslab.shinyapps.io/AuxPhos>) will be the starting
464 point of many studies that help understand the mechanistic basis of the ability of auxin to
465 control plant cell biology, physiology, growth and development.

466

467

468 **ACKNOWLEDGEMENTS**

469

470 We are grateful to Mark Estelle for making the *afb1* mutant available, our team members for
471 discussions and suggestions. This work was supported by funding from the Netherlands
472 Organization for Scientific Research (NWO): VICI grant 865.14.001 grant to D.W. and
473 VENI grant VI.VENI.212.003 to A.K.; the European Research Council AdG DIRNDL
474 (contract number 833867), StG CELLONGATE (contract 803048) to M.F. and AdG ETAP
475 (contract 742985) to J.F.; and the Austrian Science Fund (FWF, P29988) to J.F..

476

477 **AUTHOR CONTRIBUTIONS**

478

479 Conceptualization: M.R., A.K., J.F., D.W.; Methodology: M.R., S.B.; Software: S.K.M.,
480 J.K.; Formal analysis: M.R., P.K.; Investigation: M.R., A.K., P.K.; Writing – Original Draft:
481 M.R., A.K., D.W.; Writing – Review & Editing: all authors; Visualization: M.R., S.K.M.,
482 P.K.; Supervision: M.F., J.F., D.W.; Funding Acquisition: A.K., M.F., J.F., D.W..

483

484 **DECLARATION OF INTERESTS**

485

486 None of the authors have competing interest to declare.

487

488

489 **MATERIALS AND METHODS**

490

491 **Plant material, growth and treatments**

492 Arabidopsis seeds were surfaced sterilized, stratified in 0.1% agarose and grown on top of a
493 100 μ m nylon mesh on half-strength Murashige and Skoog (MS) medium with 0.8% Agar
494 (Duchefa). Seedlings were vertically grown in a growth chamber at 22 °C under long days
495 (16h:8h light:dark) for 5 days. For rapid auxin treatment, 100 nM IAA (dissolved in DMSO)
496 or an equal volume of DMSO was diluted in liquid half-strength MS medium. Plates were
497 treated one at a time, placed horizontally, and solution was slowly added until roots were
498 submerged. Plates were subsequently placed vertically again, to minimize gravitropic
499 stimulation. Roots were harvested by scalpel and directly frozen in liquid nitrogen. Roots
500 were ground to a fine powder and kept at -80 °C until further processing. For comparisons
501 between chemicals, timepoints and genotypes, all replicates of all treatments were grown on
502 the same day and processed independently.

503 Columbia-0 was used as wild-type in all experiments. Mutants used were *abp1-TD*⁶⁰,
504 *tmk1-1*⁵⁴, *afb1-3*⁶¹ and *aux1-100*⁶². For Calcium imaging, a line expressing the R-GECO1
505 sensor was used⁴⁸.

506

507 **Chemicals**

508 For microscopy, IAA (10 mM stock in 96% ethanol; Sigma Aldrich), HPTS (8-
509 Hydroxypyrene-1,3,6-Trisulfonic Acid, Trisodium Salt, 100 mM stock in water; Thermo
510 Fisher Scientific, H348) were used. For phosphoproteomics, IAA (10 mM stock in DMSO;
511 Alfa Aesar), 1-NAA (10 mM stock in DMSO; Sigma Aldrich), 2-NAA (10 mM stock in
512 DMSO; Sigma Aldrich), Benzoic acid (10 mM stock in water; Sigma Aldrich), Formic Acid
513 (10 mM stock in water; Sigma Aldrich) and Fusicoccin (1 mM stock in 96% ethanol;
514 Sigma Aldrich) were used.

515

516 **Phosphopeptide enrichment**

517 For phosphopeptide enrichment, ground Arabidopsis roots powder was suspended in an
518 extraction buffer with 100 mM Tris-HCl pH 8.0, 7 M Urea, 1% Triton-X, 10 mM DTT, 10
519 U/ml DNase I (Roche), 1 mM MgCl₂, 1% benzonase (Novagen), 1xphosphoSTOP (Pierce)
520 and 1x cocktail protease inhibitor (Pierce). The suspended lysate was sonicated using a
521 cooled (4°C) waterbath sonicator (Qsonica) using 30 cycles of 30 seconds ON and 30
522 seconds OFF at 90% amplitude. Lysate was subsequently spun down using a cooled (4°C)

523 tabletop centrifuge at 20.000xg for 30 minutes. After centrifugation supernatant was collected
524 and an extra 1% (v:v) of benzonase was added and incubated for 30 minutes at room
525 temperature. Acrylamide was added to 50 mM and incubated for an extra 30 minutes at room
526 temperature. After alkylation, proteins were precipitated using methanol/chloroform. To the
527 lysate, 4 volumes of methanol, 1 volume of chloroform and 3 volumes of milliQ was added
528 with rigorous vortexing in between. Lysate was centrifuged for 10 minutes at 5000 rpm. After
529 centrifugation, the top layer was discarded and 3 volumes of methanol were added to further
530 precipitate the protein layer by centrifugation for 10 minutes at 5000 rpm. After
531 centrifugation, the supernatant was discarded and protein pellet was air dried. Proteins were
532 next resuspended in 50 mM ammonium bicarbonate (ABC) and sonicated using a cooled
533 (4°C) waterbath sonicator (Qsonica) using 30 cycles of 30 seconds ON and 30 seconds OFF
534 at 90% amplitude. After sonication, protein concentration was measured by Bradford reagent
535 (Biorad). For every biological replicate 500 µg protein was digested with sequencing grade
536 trypsin (1:100 trypsin:protein; Roche) overnight at room temperature. Next, peptides were
537 desalted and concentrated using home-made C18 microcolumns. For peptide desalting and
538 concentrating, disposable 1000 µl pipette tips were fitted with 4 plugs of C18 octadecyl 47
539 mm Disks 2215 (Empore™) material and 1 mg:10 µg of LiChroprep® RP-18 (Merck) :
540 peptides. Tips were sequentially washed with 100 % methanol, 80 % Acetonitrile (CAN) in
541 0.1% formic acid and twice equilibrated with 0.1 % formic acid. All chromatographic steps
542 were performed by centrifugation for 4 minutes at 1500xg. After equilibration, peptides were
543 loaded for 20 minutes at 400xg. Bound peptides were washed with 0.1% formic acid and
544 eluted with 80 % ACN in 0.1 % formic acid for 4 minutes at 1500xg. Eluted peptides were
545 suspended in loading buffer (80 % acetonitrile, 5 % tri-fluor acetic acid (TFA)). For
546 phosphopeptide enrichment, MagReSyn® Ti-IMAC beads (Resyn bioscience) were used. For
547 every reaction, a 1:4 peptide:bead ratio was used. Beads were equilibrated in loading buffer,
548 resuspended peptides were added and incubated for 20 minutes at room temperature with
549 slow mixing. After 20 minutes, bead-bound phosphopeptides were washed once in loading
550 buffer, once in 80 % acetonitrile, 1 % TFA, and once in 10 % acetonitrile, 0.2 % TFA. After
551 washing, phosphopeptides were eluted twice with x ul 1 % NH₄OH. After the last elution,
552 phosphopeptides were acidified using 10 % formic acid. Phosphopeptides were subsequently
553 concentrated using home-made C18 microcolumns. For peptide desalting and concentrating,
554 disposable 200 µl pipette tips were fitted with 2 plugs of C18 octadecyl 47 mm Disks 2215
555 (Empore™) material and 1mg:10 µg of LiChroprep® RP-18 (Merck) : peptides. Tips were
556 sequentially washed and equilibrated as described above. After equilibration, peptides were

557 loaded for 20 minutes at 400xg. Bound peptides were washed with 0.1 % formic acid and
558 eluted with 80 % ACN in 0.1 % formic acid for 4 min at 1500xg. Eluted peptides were
559 subsequently concentrated using a vacuum concentrator for 30-60 minutes at 45°C and
560 resuspended in 15µl of 0.1 % formic acid.

561

562 **Filter aided sample preparation and peptide fractionation**

563 For FASP 30kDa cut-off amicon filter units (Merck Millipore) were used. Filters were first
564 washed by applying 50µl urea buffer UT buffer (8M Urea and 100mM Tris pH8.5) and
565 centrifuging for 10 minutes on 11000 RPM at 20°C. The desired amount of protein sample
566 (100µg) was next mixed with UT buffer until a volume of 200 µl, applied to the filter and
567 centrifuged for 15 minutes on 11000 RPM at 20°C. Filter was washed with UT buffer by
568 centrifugation for 15 minutes on 11000RPM at 20°C. Retained proteins were alkylated with
569 50mM acrylamide (Sigma) in UT buffer for 30 minutes at 20°C while gently shaking. Filter
570 was centrifuged and after that washed trice with UT buffer for 15 minutes on 11000RPM at
571 20°C. Next filter was washed trice in 50mM ABC buffer. After last wash proteins were
572 cleaved by adding sequencing grade trypsin (Roche) in a 1:100 trypsin:protein ratio.
573 Digestion was completed overnight. The following day the filter was placed into a new tube
574 and peptides were eluted by centrifuging for 15 minutes on 11000RPM at 20°C. Further
575 elution was completed by adding two times 50mM ABC buffer and centrifuging for 10
576 minutes on 11000RPM at 20°C.

577 FASP digested peptides (10 µg) were submitted to offline in stage-tip high pH reversed phase
578 (Hp-RP) fractionation. For Hp-RP tips, 2 plugs of C18 octadecyl 47mm Disks 2215
579 (EmporeTM) material and 1mg:10 µg of LiChroprep® RP-18 (Merck) : peptide were added to
580 a 200 µl tip. Tips were washed with methanol for 4 minutes at 1000xg. Next buffer
581 containing 0.1% formic acid and 80% acetonitrile was added and centrifuged for 4 minutes at
582 1000xg. Final equilibration was achieved with two washes of 0.1% formic acid and two
583 washes of 20mM ammonium formate (Optima®) pH10 for 4 minutes at 1000xg. Peptides
584 were suspended in 20mM ammonium formate pH10 before loading onto Hp-RP tip. Sample
585 was loaded by centrifugation for 20 minutes at 400xg. Peptides were subsequently eluted
586 with ammonium formate buffers containing 5%,8%,11%,18% and 40% ACN.

587

588 **Mass spectrometry**

589 For nano liquid chromatography–tandem mass spectrometry (LC–MS/MS) analysis 5 ul of
590 peptide samples were loaded directly onto a 0.10 * 250 mm ReproSil-Pur 120 C18-AQ 1.9

591 μ m beads analytical column (prepared in-house) at a constant pressure of 825 bar (flow rate
592 of circa 700 nL/min) with 1 ml/l HCOOH in water and eluted at a flow of 0.5 μ l/min with a
593 50 min linear gradient from 9% to 34% acetonitril in water with 1 ml/l formic acid with a
594 Thermo EASY nanoLC1000. An electrospray potential of 3.5 kV was applied directly to the
595 eluent via a stainless steel needle fitted into the waste line of a micro cross that was
596 connected between the nLC and the analytical column. Full scan positive mode FTMS
597 spectra were measured between m/z 380 and 1400 on a Exploris 480 (Thermo electron, San
598 Jose, CA, USA) in the Orbitrap at resolution (60000). MS and MSMS AGC targets were set
599 to 300%, 100% respectively or maximum ion injection times of 50 ms (MS) and 30 ms
600 (MSMS) were used. HCD fragmented (Isolation width 1.2 m/z, 28% normalized collision
601 energy) MSMS scans of 2-5+ charged peaks in the MS scan were recorded in data dependent
602 mode in a cycle time of 1.1 s (Resolution 15000, threshold 2e4, 15 s exclusion duration for
603 the selected m/z +/- 10 ppm).

604 The MaxQuant quantitative proteomics software package was used to analyse LC–MS data
605 with all MS/MS spectra. The following settings were used: peptide and protein
606 FDR ≤ 0.01 ; the proteome of *A. thaliana* (UniProt ID UP000006548) was used as the
607 protein database; maximum missed cleavage was set at 2; variable modifications Oxidation
608 (M), Acetyl (protein N-term), Deamidation (NQ), pPhospho (STY); fixed modification
609 AcrylAmide (C); match between runs and label-free quantification options were selected.

610

611

612 **Data analysis**

613 Maxquant output was analyzed using Perseus or R. For time series analysis, the Maxquant
614 output PhosphoSTY tab was imported in Perseus ⁶³. Data was filtered for reverse,
615 contaminants, only identified by site and localization probability of ≥ 0.75 . Intensity values
616 were log2 transformed and filtered to contain at least 75% valid values in one group. Values
617 were subsequently normalized by median column subtraction. Remaining missing values
618 were imputed from a normal distribution using standard settings in Perseus (width: 0.3, down
619 shift: 1.8) (Figure S2A,B). An FDR permutation based ANOVA test was performed to
620 identify significantly changing phosphosite profiles (FDR ≤ 0.01). To adjust for treatment
621 response, all log2 transformed profiles from mock treatments were merged with the auxin
622 responsive profiles. Mock values were subsequently subtracted from auxin responsive
623 profiles to obtain normalized auxin responsive phosphosite profiles.

624 Next, temporal ordering/cluster identification of the phosphosite profiles were done
625 using the Minardo-Model in R⁴⁴. Cluster number was determined in a way that most profiles
626 followed the cluster centroid, resulting in 24 clusters.

627 Gene ontology enrichment was performed using the database for annotation,
628 visualization and integrated discovery (DAVID)^{64,65}. For this, UniProt accession codes were
629 used with duplicates removed. As a background, the full *Arabidopsis thaliana* proteome was
630 used. Next REVIGO⁶⁶ and R were used to reduce overlapping GO-terms.

631 For kinase network analysis, log2-transformed phosphosite profiles of kinases with
632 phosphosites in the activation loop (as described in⁶⁷) were compared against all FDR
633 significant (FDR≤0.01) profiles using Pearson correlation and Euclidean distance (to also
634 include time offset profiles). Profiles passing a Pearson correlation threshold of ≥0.6 and
635 Euclidian distance threshold of ≤2.5 were extracted for further network analysis. For
636 network analysis, UniProt accession codes were taken as an input for Cytoscape. Network
637 analysis was performed in Cytoscape using standard settings. The degree and betweenness
638 centrality were used to determine signaling hub importance.

639 Adobe illustrator and R, using standard packages, were used for visualization.

640

641 **R shiny app**

642 All the phosphosites and the corresponding enrichment data have been imported into the R
643 environment as CSV files. DataTables, reshape2 and dplyr packages were used for data
644 visualization and data wrangling. 3D protein structures of *Arabidopsis thaliana* proteome
645 predicted through the AlphaFold2 program were downloaded from the AlphaFold database
646 hosted at EBI (<https://alphafold.ebi.ac.uk/download>). These structures were rendered and
647 visualized using the r3dmol package while the plots were generated using ggplot2 package in
648 R.

649

650 **Microfluidics experiments**

651 Four-day-old seedlings were placed into a closable microfluidic chip equipped with
652 hydraulic valves and closed by a microscopy cover glass¹⁴. One channel contained a control
653 solution (non-buffered 1/2 MS, 100 μM HPTS). The second channel contained a treatment
654 solution (non-buffered ½ MS, 100 μM HPTS, 100 nM IAA). Media flow rate was set to 3
655 μl/min (OBI1, MFS2 Elveflow and Elveflow software ESI (v.3.04.1). This system was placed
656 to a vertical microscope stage and left for 15 min plant recovery.

657

658 **Microscopy imaging**

659 Imaging was performed using a vertical stage Zeiss Axio Observer 7 coupled to a Yokogawa
660 CSU-W1-T2 spinning disk unit with 50 μm pinholes, equipped with a VS-HOM1000
661 excitation light homogenizer (Visitron Systems). Images were acquired using VisiView
662 software (Visitron Systems, v.4.4.0.14). We used a Zeiss Plan-Apochromat $\times 10/0.45$
663 objective. HPTS was excited by a 488 nm laser and R-GECO1 by a 561 nm laser. The signal
664 was detected using a PRIME-95B Back-Illuminated sCMOS camera (1,200 \times 1,200 pixels;
665 Photometrics). The seedlings were imaged every 10 seconds for a duration of 10 minutes.

666

667 **Image analysis**

668 The microscopy images were analyzed in ImageJ Fiji software⁶⁸. HPTS signal intensity was
669 measured using rectangular selection in an area on the outer surface of the root, individually
670 along both sides of the root elongation zone. The intensity of the background was measured
671 using rectangular selection in areas not affected by root response and subtracted from the root
672 sides values. For analysis, the average of the values from both root sides was used. The signal
673 intensity of R-GECO1 was measured in a rectangular selection inside the root at the root
674 elongation zone. Due to the high heterogeneity of the samples, the datasets were normalized
675 using division by initial fluorescence intensity values (F/F0). As initial value F0, we used the
676 average fluorescence intensity at five time points before treatment.

677

678 **Data availability**

679 The mass spectrometry proteomics data, protein lists and intensity values of all samples have
680 been deposited to the ProteomeXchange Consortium via the PRIDE⁶⁹ partner repository with
681 the dataset identifier XXX. Source code and complete data used in AuxPhos is available on
682 GitHub (<https://github.com/WeijersLab/AuxPhos>), while the webtool is accessible from
683 Shinyapps server (<https://weijerslab.shinyapps.io/AuxPhos>).

684

685

686

687

688 **REFERENCES**

689

- 690 1. Went, F.W. (1928). Wuchsstoff und Wachstum. *Recueil des travaux botaniques*
691 néerlandais 25, 1–116.
- 692 2. Went, F.W., and Thimann, K.V. (1937). *Phytohormones* (MacMillan Company).
- 693 3. Friml, J. (2022). Fourteen Stations of Auxin. *Cold Spring Harb Perspect Biol* 14,
694 a039859. 10.1101/cshperspect.a039859.
- 695 4. Morffy, N., and Strader, L.C. (2020). Old Town Roads: routes of auxin biosynthesis
696 across kingdoms. *Curr Opin Plant Biol* 55, 21–27. 10.1016/j.pbi.2020.02.002.
- 697 5. Friml, J., Wiśniewska, J., Benková, E., Mendgen, K., and Palme, K. (2002). Lateral
698 relocation of auxin efflux regulator PIN3 mediates tropism in *Arabidopsis*. *Nature* 415,
699 806–809. 10.1038/415806a.
- 700 6. Tao, Y., Ferrer, J.-L., Ljung, K., Pojer, F., Hong, F., Long, J.A., Li, L., Moreno, J.E.,
701 Bowman, M.E., Ivans, L.J., et al. (2008). Rapid Synthesis of Auxin via a New
702 Tryptophan-Dependent Pathway Is Required for Shade Avoidance in Plants. *Cell* 133,
703 164–176. 10.1016/j.cell.2008.01.049.
- 704 7. Scarpella, E., Marcos, D., Friml, J., and Berleth, T. (2006). Control of leaf vascular
705 patterning by polar auxin transport. *Genes Dev* 20, 1015–1027.
706 10.1101/gad.1402406.
- 707 8. de Rybel, B., Adibi, M., Breda, A.S., Wendrich, J.R., Smit, M.E., Novák, O., Yamaguchi,
708 N., Yoshida, S., van Isterdael, G., Palovaara, J., et al. (2014). Integration of growth and
709 patterning during vascular tissue formation in *Arabidopsis*. *Science* (1979) 345.
710 10.1126/science.1255215.
- 711 9. Sachs, T. (2000). Integrating Cellular and Organismic Aspects of Vascular
712 Differentiation. *Plant Cell Physiol* 41, 649–656. 10.1093/pcp/41.6.649.
- 713 10. Casimiro, I., Marchant, A., Bhalerao, R.P., Beeckman, T., Dhooge, S., Swarup, R.,
714 Graham, N., Inzé, D., Sandberg, G., Casero, P.J., et al. (2001). Auxin Transport
715 Promotes *Arabidopsis* Lateral Root Initiation. *Plant Cell* 13, 843–852.
716 10.1105/tpc.13.4.843.
- 717 11. Dubrovsky, J.G., Sauer, M., Napsucialy-Mendivil, S., Ivanchenko, M.G., Friml, J.,
718 Shishkova, S., Celenza, J., and Benková, E. (2008). Auxin acts as a local morphogenetic
719 trigger to specify lateral root founder cells. *Proceedings of the National Academy of
720 Sciences* 105, 8790–8794. 10.1073/pnas.0712307105.
- 721 12. Bates, G.W., and Goldsmith, M.H.M. (1983). Rapid response of the plasma-membrane
722 potential in oat coleoptiles to auxin and other weak acids. *Planta* 159, 231–237.
723 10.1007/BF00397530.
- 724 13. Etherton, B. (1970). Effect of Indole-3-acetic Acid on Membrane Potentials of Oat
725 Coleoptile Cells. *Plant Physiol* 45, 527–528. 10.1104/pp.45.4.527.
- 726 14. Serre, N.B.C., Kralík, D., Yun, P., Slouka, Z., Shabala, S., and Fendrych, M. (2021). AFB1
727 controls rapid auxin signalling through membrane depolarization in *Arabidopsis*
728 *thaliana* root. *Nat Plants* 7, 1229–1238. 10.1038/s41477-021-00969-z.
- 729 15. Monshausen, G.B., Miller, N.D., Murphy, A.S., and Gilroy, S. (2011). Dynamics of
730 auxin-dependent Ca²⁺ and pH signaling in root growth revealed by integrating high-
731 resolution imaging with automated computer vision-based analysis. *The Plant Journal*
732 65, 309–318. 10.1111/j.1365-313X.2010.04423.x.

733 16. Friml, J., Gallei, M., Gelová, Z., Johnson, A., Mazur, E., Monzer, A., Rodriguez, L.,
734 Roosjen, M., Verstraeten, I., Živanović, B.D., et al. (2022). ABP1-TMK auxin perception
735 for global phosphorylation and auxin canalization. *Nature* **609**, 575–581.
736 10.1038/s41586-022-05187-x.

737 17. Ayling, S., and Clarkson, D. (1996). The Cytoplasmic Streaming Response of Tomato
738 Root Hairs to Auxin; the Role of Calcium. *Functional Plant Biology* **23**, 699.
739 10.1071/PP9960699.

740 18. Thimann, K. v. (1938). HORMONES AND THE ANALYSIS OF GROWTH. *Plant Physiol* **13**,
741 437–449. 10.1104/pp.13.3.437.

742 19. Reinhardt, D., Pesce, E.-R., Stieger, P., Mandel, T., Baltensperger, K., Bennett, M.,
743 Traas, J., Friml, J., and Kuhlemeier, C. (2003). Regulation of phyllotaxis by polar auxin
744 transport. *Nature* **426**, 255–260. 10.1038/nature02081.

745 20. Heisler, M.G., Ohno, C., Das, P., Sieber, P., Reddy, G. v., Long, J.A., and Meyerowitz,
746 E.M. (2005). Patterns of Auxin Transport and Gene Expression during Primordium
747 Development Revealed by Live Imaging of the *Arabidopsis* Inflorescence Meristem.
748 *Current Biology* **15**, 1899–1911. 10.1016/j.cub.2005.09.052.

749 21. Weijers, D., and Wagner, D. (2016). Transcriptional Responses to the Auxin Hormone.
750 *Annu Rev Plant Biol* **67**, 539–574. 10.1146/annurev-arplant-043015-112122.

751 22. Leyser, H.M.O., Lincoln, C.A., Timpte, C., Lammer, D., Turner, J., and Estelle, M.
752 (1993). *Arabidopsis* auxin-resistance gene AXR1 encodes a protein related to
753 ubiquitin-activating enzyme E1. *Nature* **364**, 161–164. 10.1038/364161a0.

754 23. Hobbie, L., and Estelle, M. (1995). The axr4 auxin-resistant mutants of *Arabidopsis*
755 thaliana define a gene important for root gravitropism and lateral root initiation. *The
756 Plant Journal* **7**, 211–220. 10.1046/j.1365-313X.1995.7020211.x.

757 24. Leyser, O. (1997). Auxin: Lessons from a mutant weed. *Physiol Plant* **100**, 407–414.
758 <https://doi.org/10.1111/j.1399-3054.1997.tb03044.x>.

759 25. Abel, S., and Theologis, A. (1996). Early Genes and Auxin Action. *Plant Physiol* **111**, 9–
760 17. 10.1104/pp.111.1.9.

761 26. Dindas, J., Scherzer, S., Roelfsema, M.R.G., von Meyer, K., Müller, H.M., Al-Rasheid,
762 K.A.S., Palme, K., Dietrich, P., Becker, D., Bennett, M.J., et al. (2018). AUX1-mediated
763 root hair auxin influx governs SCFTIR1/AFB-type Ca²⁺ signaling. *Nat Commun* **9**, 1174.
764 10.1038/s41467-018-03582-5.

765 27. Li, L., Verstraeten, I., Roosjen, M., Takahashi, K., Rodriguez, L., Merrin, J., Chen, J.,
766 Shabala, L., Smet, W., Ren, H., et al. (2021). Cell surface and intracellular auxin
767 signalling for H⁺ fluxes in root growth. *Nature* **599**, 273–277. 10.1038/s41586-021-
768 04037-6.

769 28. Fendrych, M., Akhmanova, M., Merrin, J., Glanc, M., Hagiwara, S., Takahashi, K.,
770 Uchida, N., Torii, K.U., and Friml, J. (2018). Rapid and reversible root growth inhibition
771 by TIR1 auxin signalling. *Nat Plants* **4**, 453–459. 10.1038/s41477-018-0190-1.

772 29. Lin, W., Zhou, X., Tang, W., Takahashi, K., Pan, X., Dai, J., Ren, H., Zhu, X., Pan, S.,
773 Zheng, H., et al. (2021). TMK-based cell-surface auxin signalling activates cell-wall
774 acidification. *Nature* **599**, 278–282. 10.1038/s41586-021-03976-4.

775 30. Narasimhan, M., Gallei, M., Tan, S., Johnson, A., Verstraeten, I., Li, L., Rodriguez, L.,
776 Han, H., Himschoot, E., Wang, R., et al. (2021). Systematic analysis of specific and
777 nonspecific auxin effects on endocytosis and trafficking. *Plant Physiol* **186**, 1122–
778 1142. 10.1093/plphys/kiab134.

779 31. Jin, J., and Pawson, T. (2012). Modular evolution of phosphorylation-based signalling
780 systems. *Philosophical Transactions of the Royal Society B: Biological Sciences* **367**,
781 2540–2555. 10.1098/rstb.2012.0106.

782 32. Nurnberger, T., Brunner, F., Kemmerling, B., and Piater, L. (2004). Innate immunity in
783 plants and animals: striking similarities and obvious differences. *Immunol Rev* **198**,
784 249–266. 10.1111/j.0105-2896.2004.0119.x.

785 33. Couto, D., and Zipfel, C. (2016). Regulation of pattern recognition receptor signalling
786 in plants. *Nat Rev Immunol* **16**, 537–552. 10.1038/nri.2016.77.

787 34. Oyama, M., Kozuka-Hata, H., Tasaki, S., Semba, K., Hattori, S., Sugano, S., Inoue, J.,
788 and Yamamoto, T. (2009). Temporal Perturbation of Tyrosine Phosphoproteome
789 Dynamics Reveals the System-wide Regulatory Networks. *Molecular & Cellular
790 Proteomics* **8**, 226–231. 10.1074/mcp.M800186-MCP200.

791 35. Humphrey, S.J., Azimifar, S.B., and Mann, M. (2015). High-throughput
792 phosphoproteomics reveals in vivo insulin signaling dynamics. *Nat Biotechnol* **33**,
793 990–995. 10.1038/nbt.3327.

794 36. Kinoshita, T., Caño-Delgado, A., Seto, H., Hiranuma, S., Fujioka, S., Yoshida, S., and
795 Chory, J. (2005). Binding of brassinosteroids to the extracellular domain of plant
796 receptor kinase BRI1. *Nature* **433**, 167–171. 10.1038/nature03227.

797 37. Wang, X., Kota, U., He, K., Blackburn, K., Li, J., Goshe, M.B., Huber, S.C., and Clouse,
798 S.D. (2008). Sequential Transphosphorylation of the BRI1/BAK1 Receptor Kinase
799 Complex Impacts Early Events in Brassinosteroid Signaling. *Dev Cell* **15**, 220–235.
800 10.1016/j.devcel.2008.06.011.

801 38. Ryu, H., Kim, K., Cho, H., Park, J., Choe, S., and Hwang, I. (2007). Nucleocytoplasmic
802 Shuttling of BZR1 Mediated by Phosphorylation Is Essential in *Arabidopsis*
803 Brassinosteroid Signaling. *Plant Cell* **19**, 2749–2762. 10.1105/tpc.107.053728.

804 39. Tan, S., Luschnig, C., and Friml, J. (2021). Pho-view of Auxin: Reversible Protein
805 Phosphorylation in Auxin Biosynthesis, Transport and Signaling. *Mol Plant* **14**, 151–
806 165. 10.1016/j.molp.2020.11.004.

807 40. Zhang, H., Zhou, H., Berke, L., Heck, A.J.R., Mohammed, S., Scheres, B., and Menke,
808 F.L.H. (2013). Quantitative Phosphoproteomics after Auxin-stimulated Lateral Root
809 Induction Identifies an SNX1 Protein Phosphorylation Site Required for Growth.
810 *Molecular & Cellular Proteomics* **12**, 1158–1169. 10.1074/mcp.M112.021220.

811 41. Nikonorova, N., Murphy, E., Fonseca de Lima, C.F., Zhu, S., van de Cotte, B., Vu, L.D.,
812 Balcerowicz, D., Li, L., Kong, X., de Rop, G., et al. (2021). The *Arabidopsis* Root Tip
813 (Phospho)Proteomes at Growth-Promoting versus Growth-Repressing Conditions
814 Reveal Novel Root Growth Regulators. *Cells* **10**, 1665. 10.3390/cells10071665.

815 42. Singh, H., Singh, Z., Zhu, T., Xu, X., Waghmode, B., Garg, T., Yadav, S., Sircar, D., de
816 Smet, I., and Yadav, S.R. (2021). Auxin-Responsive (Phospho)proteome Analysis
817 Reveals Key Biological Processes and Signaling Associated with Shoot-Borne Crown
818 Root Development in Rice. *Plant Cell Physiol.* 10.1093/pcp/pcab155.

819 43. McClure, B.A., Hagen, G., Brown, C.S., Gee, M.A., and Guilfoyle, T.J. (1989).
820 Transcription, organization, and sequence of an auxin-regulated gene cluster in
821 soybean. *Plant Cell* **1**, 229–239. 10.1105/tpc.1.2.229.

822 44. Kaur, S., Peters, T.J., Yang, P., Luu, L.D.W., Vuong, J., Krycer, J.R., and O'Donoghue, S.I.
823 (2020). Temporal ordering of omics and multiomic events inferred from time-series
824 data. *NPJ Syst Biol Appl* **6**, 22. 10.1038/s41540-020-0141-0.

825 45. Yang, Y., Hammes, U.Z., Taylor, C.G., Schachtman, D.P., and Nielsen, E. (2006). High-
826 Affinity Auxin Transport by the AUX1 Influx Carrier Protein. *Current Biology* **16**, 1123–
827 1127. 10.1016/j.cub.2006.04.029.

828 46. Weller, B., Zourelidou, M., Frank, L., Barbosa, I.C.R., Fastner, A., Richter, S., Jürgens,
829 G., Hammes, U.Z., and Schwechheimer, C. (2017). Dynamic PIN-FORMED auxin efflux
830 carrier phosphorylation at the plasma membrane controls auxin efflux-dependent
831 growth. *Proceedings of the National Academy of Sciences* **114**.
832 10.1073/pnas.1614380114.

833 47. Barbez, E., Dünser, K., Gaidora, A., Lendl, T., and Busch, W. (2017). Auxin steers root
834 cell expansion via apoplastic pH regulation in *Arabidopsis thaliana*. *Proceedings of the*
835 *National Academy of Sciences* **114**. 10.1073/pnas.1613499114.

836 48. Keinath, N.F., Waadt, R., Brugman, R., Schroeder, J.I., Grossmann, G., Schumacher, K.,
837 and Krebs, M. (2015). Live Cell Imaging with R-GECO1 Sheds Light on flg22- and
838 Chitin-Induced Transient [Ca(2+)]_{cyt} Patterns in *Arabidopsis*. *Mol Plant* **8**, 1188–1200.
839 10.1016/j.molp.2015.05.006.

840 49. Behera, S., Zhaolong, X., Luoni, L., Bonza, M.C., Docula, F.G., de Michelis, M.I.,
841 Morris, R.J., Schwarländer, M., and Costa, A. (2018). Cellular Ca²⁺ Signals Generate
842 Defined pH Signatures in Plants. *Plant Cell* **30**, 2704–2719. 10.1105/tpc.18.00655.

843 50. Olsson, A., Svennelid, F., Ek, B., Sommarin, M., and Larsson, C. (1998). A
844 Phosphothreonine Residue at the C-Terminal End of the Plasma Membrane H⁺-
845 ATPase Is Protected by Fusicoccin-Induced 14–3–3 Binding. *Plant Physiol* **118**, 551–
846 555. 10.1104/pp.118.2.551.

847 51. Wang, Y., Goertz, N.J., Rillo, E., and Yang, M. (2022). Negative regulation of seed
848 germination by maternal AFB1 and AFB5 in *Arabidopsis*. *Biosci Rep* **42**.
849 10.1042/BSR20221504.

850 52. Svennelid, F., Olsson, A., Piotrowski, M., Rosenquist, M., Ottman, C., Larsson, C.,
851 Oecking, C., and Sommarin, M. (1999). Phosphorylation of Thr-948 at the C Terminus
852 of the Plasma Membrane H⁺-ATPase Creates a Binding Site for the Regulatory 14-3-3
853 Protein. *Plant Cell* **11**, 2379–2391. 10.1105/tpc.11.12.2379.

854 53. Gelová, Z., Gallei, M., Pernisová, M., Brunoud, G., Zhang, X., Glanc, M., Li, L.,
855 Michalko, J., Pavlovičová, Z., Verstraeten, I., et al. (2021). Developmental roles of
856 Auxin Binding Protein 1 in *Arabidopsis thaliana*. *Plant Science* **303**, 110750.
857 10.1016/j.plantsci.2020.110750.

858 54. Dai, N., Wang, W., Patterson, S.E., and Bleecker, A.B. (2013). The TMK Subfamily of
859 Receptor-Like Kinases in *Arabidopsis* Display an Essential Role in Growth and a
860 Reduced Sensitivity to Auxin. *PLoS One* **8**, e60990–.

861 55. Chen, R., Binder, B.M., Garrett, W.M., Tucker, M.L., Chang, C., and Cooper, B. (2011).
862 Proteomic responses in *Arabidopsis thaliana* seedlings treated with ethylene. *Mol*
863 *Biosyst* **7**, 2637. 10.1039/c1mb05159h.

864 56. Ju, C., Yoon, G.M., Shemansky, J.M., Lin, D.Y., Ying, Z.I., Chang, J., Garrett, W.M.,
865 Kessenbrock, M., Groth, G., Tucker, M.L., et al. (2012). CTR1 phosphorylates the
866 central regulator EIN2 to control ethylene hormone signaling from the ER membrane
867 to the nucleus in *Arabidopsis*. *Proceedings of the National Academy of Sciences* **109**,
868 19486–19491. 10.1073/pnas.1214848109.

869 57. Kuhn, A., Ramans Harborough, S., McLaughlin, H.M., Natarajan, B., Verstraeten, I.,
870 Friml, J., Kepinski, S., and Østergaard, L. (2020). Direct ETTIN-auxin interaction
871 controls chromatin states in gynoecium development. *Elife* **9**. 10.7554/eLife.51787.

872 58. Szemenyei, H., Hannon, M., and Long, J.A. (2008). TOPLESS Mediates Auxin-
873 Dependent Transcriptional Repression During *Arabidopsis* Embryogenesis. *Science*
874 (1979) 319, 1384–1386. 10.1126/science.1151461.

875 59. Wu, M.-F., Yamaguchi, N., Xiao, J., Bargmann, B., Estelle, M., Sang, Y., and Wagner, D.
876 (2015). Auxin-regulated chromatin switch directs acquisition of flower primordium
877 founder fate. *eLife* 4. 10.7554/eLife.09269.

878 60. Gao, Y., Zhang, Y., Zhang, D., Dai, X., Estelle, M., and Zhao, Y. (2015). Auxin binding
879 protein 1 (ABP1) is not required for either auxin signaling or *Arabidopsis*
880 development. *Proceedings of the National Academy of Sciences* 112, 2275–2280.
881 10.1073/pnas.1500365112.

882 61. Savaldi-Goldstein, S., Baiga, T.J., Pojer, F., Dabi, T., Butterfield, C., Parry, G., Santner,
883 A., Dharmasiri, N., Tao, Y., Estelle, M., et al. (2008). New auxin analogs with growth-
884 promoting effects in intact plants reveal a chemical strategy to improve hormone
885 delivery. *Proceedings of the National Academy of Sciences* 105, 15190–15195.
886 10.1073/pnas.0806324105.

887 62. Bennett, M.J., Marchant, A., Green, H.G., May, S.T., Ward, S.P., Millner, P.A., Walker,
888 A.R., Schulz, B., and Feldmann, K.A. (1996). *Arabidopsis* AUX1 Gene: A Permease-Like
889 Regulator of Root Gravitropism. *Science* (1979) 273, 948–950.
890 10.1126/science.273.5277.948.

891 63. Tyanova, S., Temu, T., Sinitcyn, P., Carlson, A., Hein, M.Y., Geiger, T., Mann, M., and
892 Cox, J. (2016). The Perseus computational platform for comprehensive analysis of
893 (prote)omics data. *Nat Methods* 13, 731–740. 10.1038/nmeth.3901.

894 64. Sherman, B.T., Hao, M., Qiu, J., Jiao, X., Baseler, M.W., Lane, H.C., Imamichi, T., and
895 Chang, W. (2022). DAVID: a web server for functional enrichment analysis and
896 functional annotation of gene lists (2021 update). *Nucleic Acids Res* 50, W216–W221.
897 10.1093/nar/gkac194.

898 65. Huang, D.W., Sherman, B.T., and Lempicki, R.A. (2009). Systematic and integrative
899 analysis of large gene lists using DAVID bioinformatics resources. *Nat Protoc* 4, 44–57.
900 10.1038/nprot.2008.211.

901 66. Supek, F., Bošnjak, M., Škunca, N., and Šmuc, T. (2011). REVIGO Summarizes and
902 Visualizes Long Lists of Gene Ontology Terms. *PLoS One* 6, e21800.
903 10.1371/journal.pone.0021800.

904 67. Montes, C., Wang, P., Liao, C., Nolan, T.M., Song, G., Clark, N.M., Elmore, J.M., Guo,
905 H., Bassham, D.C., Yin, Y., et al. (2022). Integration of multi-omics data reveals
906 interplay between brassinosteroid and Target of Rapamycin Complex signaling in
907 *Arabidopsis*. *New Phytologist* 236, 893–910. 10.1111/nph.18404.

908 68. Schindelin, J., Arganda-Carreras, I., Frise, E., Kaynig, V., Longair, M., Pietzsch, T.,
909 Preibisch, S., Rueden, C., Saalfeld, S., Schmid, B., et al. (2012). Fiji: an open-source
910 platform for biological-image analysis. *Nat Methods* 9, 676–682.
911 10.1038/nmeth.2019.

912 69. Perez-Riverol, Y., Bai, J., Bandla, C., García-Seisdedos, D., Hewapathirana, S.,
913 Kamatchinathan, S., Kundu, D.J., Prakash, A., Frericks-Zipper, A., Eisenacher, M., et al.
914 (2022). The PRIDE database resources in 2022: a hub for mass spectrometry-based
915 proteomics evidences. *Nucleic Acids Res* 50, D543–D552. 10.1093/nar/gkab1038.

916

918 **FIGURE LEGENDS**

919

920 **Figure 1: Auxin triggers a unique phosphorylation response**

921 (A) Volcano plot showing differential abundance of phosphopeptides between Arabidopsis
922 roots treated with 100 nM IAA, or mock medium for 2 minutes. Each dot represents a single
923 phosphosite, and the significance across replicates is indicated as FDR. Statistical cut-off
924 ($FDR \leq 0.05$) is indicated, and a global density histogram is plotted on top. (B) Correlation
925 between fold-changes in IAA-triggered shotgun proteome (x-axis) and phosphoproteome (y-
926 axis) both treated with 100 nM IAA for 2 minutes. Red line is regression line with confidence
927 interval (grey). (C) Correlation plot of two independent IAA phosphoproteome experiments.
928 Spearman correlation of all sites is 0.64 while it is 0.77 when considering only differential
929 sites at $FDR \leq 0.05$. (D) Plots comparing differential phosphosites ($FDR \leq 0.05$) in 2 minutes
930 100 nM IAA treatment (x-axes) with fold-change of corresponding phosphosites in similar
931 treatments with other compounds. Structures and pKa values are given for each compound.
932 Red line indicates regression line (with confidence interval in grey), and Spearman
933 correlation value is indicated in each plot.

934

935 **Figure 2: Dynamics of auxin phosphoresponse**

936 (A) Schematic overview of treatment, time and analysis procedure. Roots of Arabidopsis
937 seedlings were treated with 100 nM IAA or 1/2MS medium with DMSO as treatment control
938 for various timepoints. Datasets were individually analyzed and intensities of treatment
939 control were subtracted from the auxin responsive profiles ($FDR \geq 0.01$) resulting in
940 normalized auxin-responsive profiles. (B) Principal component analysis of normalized auxin-
941 responsive profiles and washout. (C) Principal component analysis of normalized MS1
942 phosphosite intensities of time series in the *aux1-100* mutant. (D) Time series ordering of all
943 $FDR \geq 0.01$ log2 Z-scored normalized auxin-responsive profiles using the Minardo-model.
944 Clusters are ordered based on earliest phosphorylation event. Phosphorylation event is based
945 on the median time at which all individual profiles in a cluster cross half-maximal abundance
946 within each event window (identified by the red or blue dashed line in graph and red and blue
947 arrows on x-axis, respectively).

948

949 **Figure 3: Requirements for auxin-triggered phosphorylation**

950 (A) Correlation plot of phosphosite intensity differences between *tmk1-1*, *abp1-TD1* or *afb1-3*
951 mutants and wild-type after 2 minutes treatments with 100 nM IAA, plotted against fold-

952 change of significantly (FDR ≤ 0.05) auxin-regulated in Col-0 wild-type. Opposite regulation
953 is marked in red or blue. Similar regulation in black. **(B)** Correlation plot of phosphosite
954 intensity differences between untreated *tmk1-1*, *abp1-TD1* or *afb1-3* mutants and wild-type
955 (y-axis), plotted against fold-change of significantly (FDR ≤ 0.05) auxin-regulated in Col-0
956 wild-type. **(C)** Principal component analysis of mean-normalized MS1 intensities of the 1048
957 phosphosites that are significantly (FDR ≤ 0.05) differentially regulated in 2 minutes IAA-
958 treated Col-0, in mock- and IAA-treated wild-type and *abp1*, *tmk1* and *afb1* mutants. **(D)**
959 Distribution histograms depicting fold-change (IAA/mock) of significantly regulated
960 phosphosites of *tmk1-1*, *abp1-TD1* and *afb1-3*. Dashed grey line depicts distribution in Col-0
961 wild-type. **(E)** Heatmap of z-scored normalized MS1 phosphosite intensities in *tmk1-1*, *abp1-*
962 *TD1* and *afb1-3* mutants and Col-0 wild-type of the 1048 phosphosites that are significantly
963 (FDR ≤ 0.05) differentially regulated in wild-type upon IAA treatment. **(F)** Boxplots of MS1
964 intensities of 20 phosphosites in Col-0, *tmk1-1*, *abp1-TD1*, *afb1-3* under mock (white) and 2
965 minutes 100 nM IAA conditions (blue). N.D. means not detected in any of the four biological
966 replicates. Color legend of genotypes is indicated below.
967

968 **Figure 4: Auxin targets multiple pathways**

969 **(A)** Gene ontology showing the top 20 enrichments of biological process, molecular function
970 and cellular component on the significantly (FDR ≥ 1.99) auxin-regulated. **(B)** Examples of
971 dynamics of auxin-regulated phosphosites in diverse pathways and functions. Heatmaps
972 depict normalized intensity profiles along the time series. Protein identity is given, along with
973 the position of the phosphosite. **(C)** Screenshots of the R shiny app Auxphos. Selected
974 profiles of a single protein can be selected, visualized in a plot and phosphosites can be
975 mapped on a 3D predicted protein structure using AlphaFold.
976

977 **Figure 5: Inference of kinase-substrate relationships**

978 **(A)** Schematic overview of the kinase network inference approach. Phosphosites in predicted
979 and known activation loops were selected from the time series data. The time series profile of
980 the individual activation loop phosphosites were next analysed using correlation analysis
981 (Pearson R and Euclidian distance). Profiles of phosphosites passing the threshold (Pearson R
982 ≥ 0.6 , Euclidian distance ≤ 2.5) were considered as potential substrates, and used to build a
983 network. **(B)** Heatmap depicting the normalized intensity profiles of phosphopeptides in the
984 activation loop of kinases along the time series. **(C)** Plots showing normalized
985 phosphopeptide abundance profiles along auxin time series of known kinase-substrate pairs

986 recovered in the network inference approach. **(D)** Network position of auxin-regulated
987 kinases analyzed in the inference approach. Plot depicts degree (i.e. how many
988 edges/interactions a node has) and betweenness centrality. The latter is a measurement of hub
989 importance/centrality of a node.

990

991 **Figure 6: Auxin-triggered apoplastic pH changes**

992 **(A)** Heatmap depicting Z-score normalized values of all identified AHA phosphosites, along
993 the time series, and clustered by identity of the sites. Some represent known activation or
994 inhibition sites, while others are not functionally understood (unknown). A TMK1
995 phosphosite is shown below for comparison. **(B)** Quantitative analysis of rapid apoplastic pH
996 changes (HPTS fluorescence intensity) following auxin treatment. Dotted lines represent
997 average values from both root sizes of individual roots while black lines represent average of
998 all measured roots (n=6). **(C)** Volcano plot showing phosphosites responsive to 5 minutes 1
999 μM Fusicoccin (FC) treatment, compared to mock control. **(D)** Venn diagram depicting
1000 overlap between significant (FDR ≤ 0.05) differential phosphosites in the auxin-induction
1001 time series, and the FC. **(E)** REVIGO plot (GO analysis) of the 581 phosphosites in the
1002 overlap between auxin and FC treatment. Some proteins in highlighted categories are
1003 indicated in boxes. **(F)** Quantitative analysis of calcium influx following auxin treatment in
1004 the R-GECO1 line. Dotted lines represent normalized values of individual roots while black
1005 lines represents average of all measured roots (n=6).

1006

1007 **Supplementary Figure 1: Specificity of auxin-induced phosphorylation**

1008 **(A)** Venn diagram showing overlap of differentially phosphorylated proteins after 2 minutes
1009 IAA treatment and differentially expressed genes after 1 hour of IAA treatment
1010 (transcriptome data from Kuhn-Roosjen et al., accompanying manuscript). **(B)** Plots
1011 comparing differential phosphosites (FDR ≤ 0.05) in 2 minutes 100 nM IAA treatment (x-
1012 axes) with fold-change of corresponding phosphosites in treatments with 1-NAA, 2-NAA or
1013 BA at 1 μM . Red line indicates regression line, and Spearman correlation value is indicated
1014 in each plot.

1015

1016 **Supplementary Figure 2: Global phosphoprotein properties**

1017 **(A)** Boxplots showing MS1 phosphopeptide intensity distributions across all samples in the
1018 time series dataset, and **(B)** normalized and imputed MS1 intensities showing normal
1019 distribution of data. **(C)** Principal component analysis of normalized and imputed MS1

1020 intensities show a clear distinction between treatments and the steady state phosphorylation
1021 state emphasizing the importance of using a treatment control.

1022

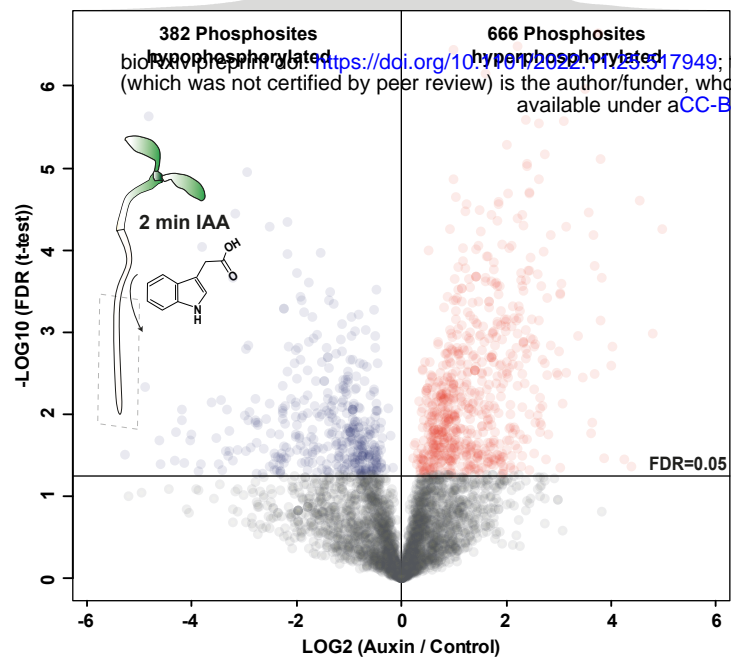
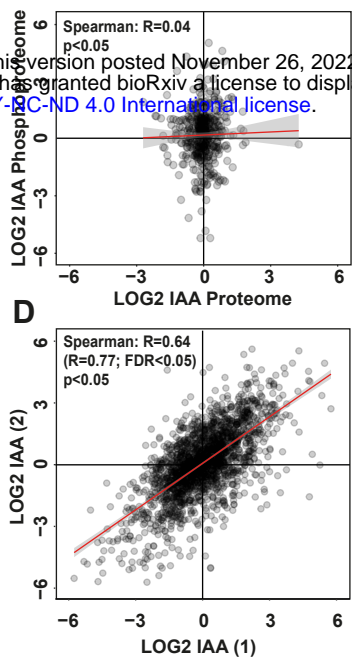
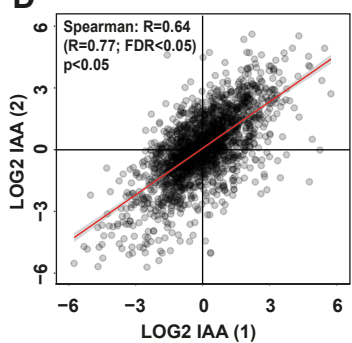
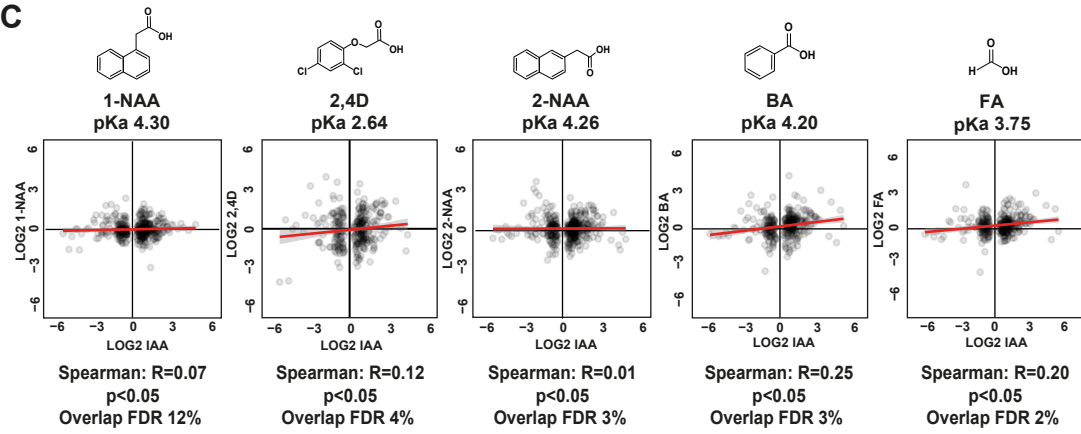
1023 **Supplementary Figure 3: Inferred kinase-substrate network**

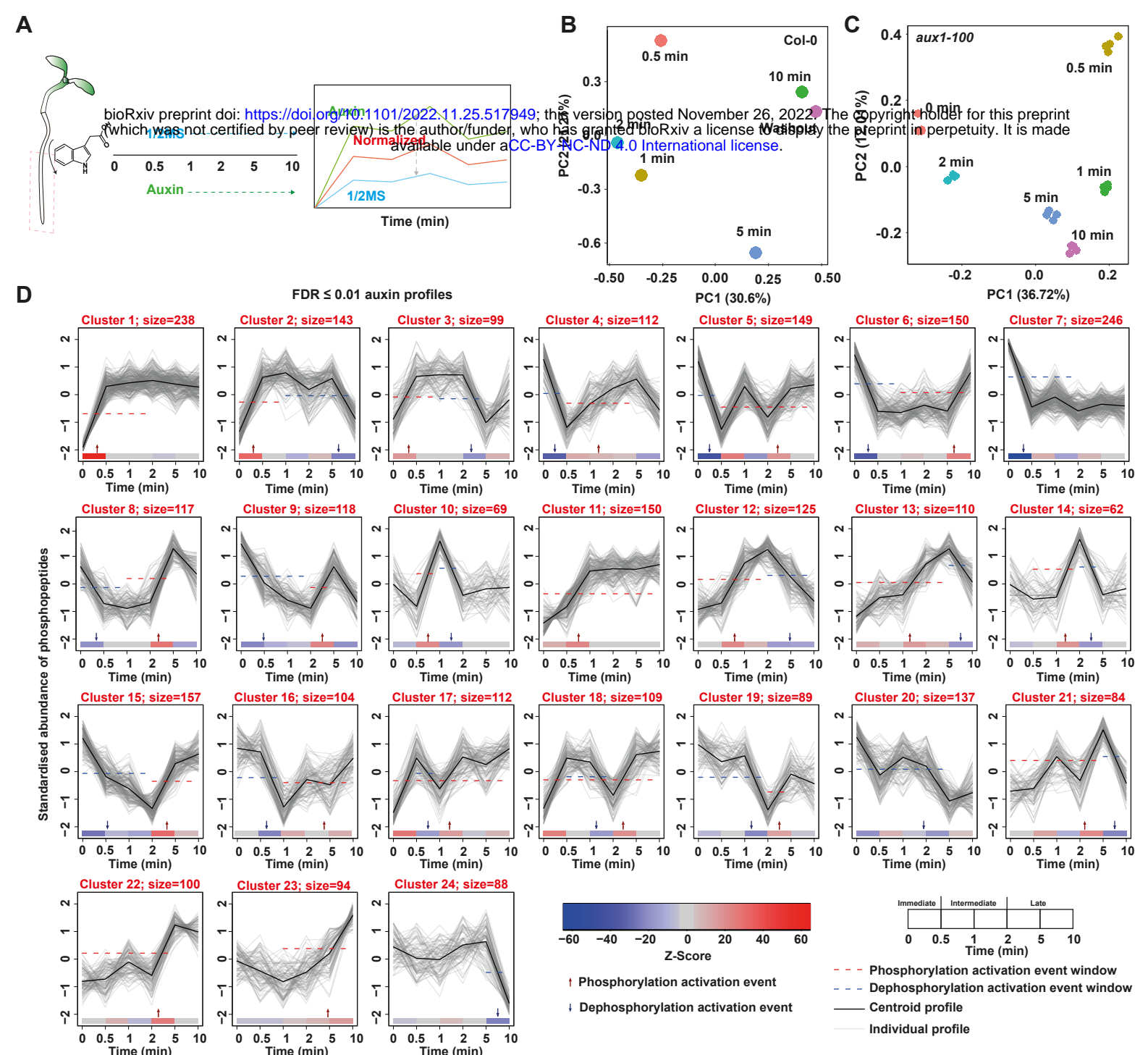
1024 Kinase network of the 23 identified kinases with phosphoregulation in their activation loop.
1025 Kinases are depicted in blue while substrates are depicted in yellow. Sizes of hexagons are
1026 based on degree.

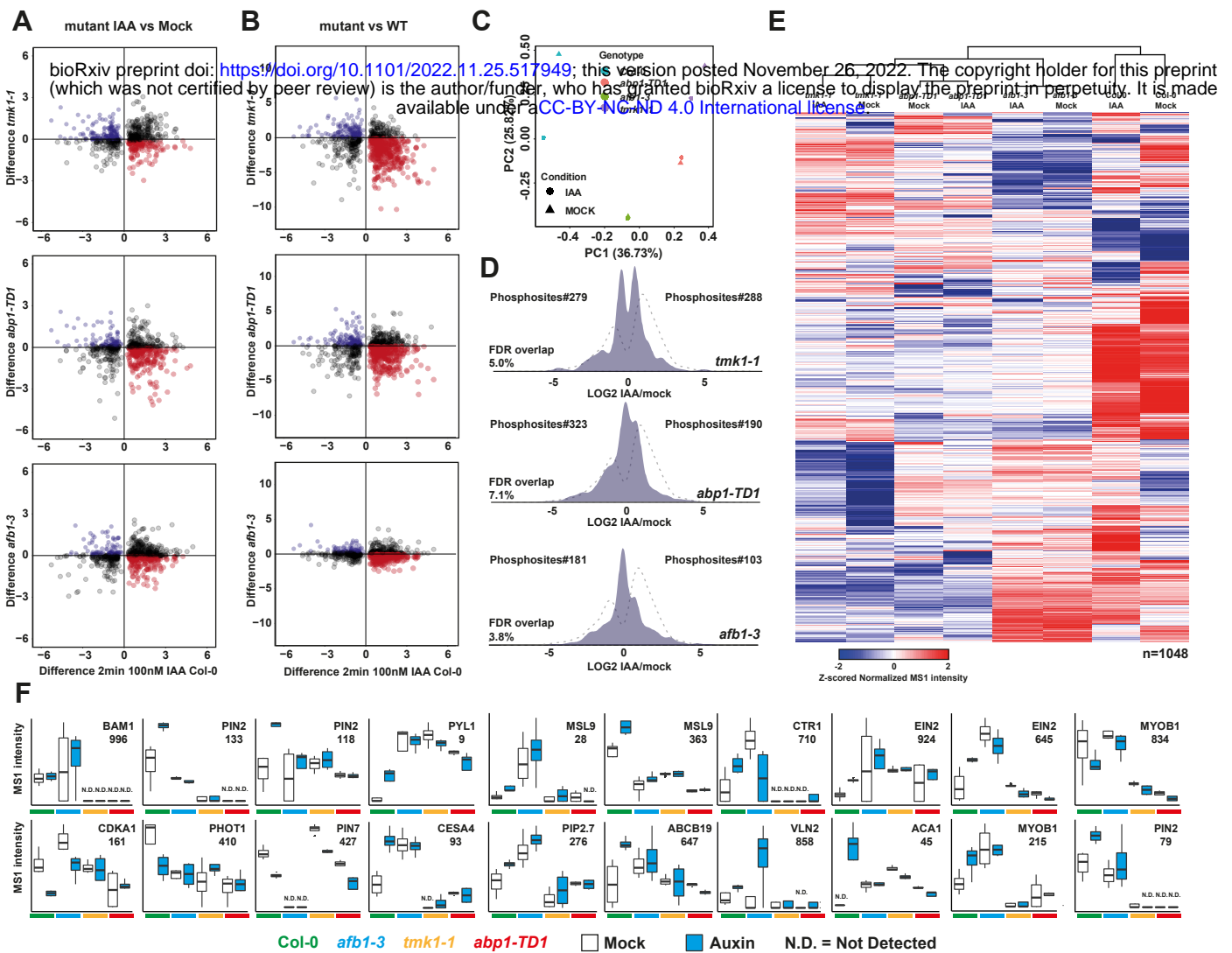
1027

1028 **Supplemental Figure 4: Effect of control medium treatment on Arabidopsis root surface
1029 pH and cytosolic Ca²⁺ level**

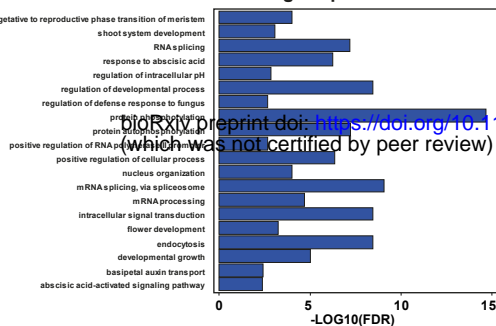
1030 (A) Root surface pH was visualized by fluorescence intensity of HPTS 488 nm pH-
1031 responsive channel. (B) The level of cytoplasmic Ca²⁺ was reported by the fluorescence
1032 intensity of R-GECO1. Treatment is indicated by the vertical dotted line (n=3 roots). (C)
1033 Fluorescence intensity of HPTS 488 nm channel and R-GECO1 was measured in the
1034 rectangular regions near the root surface (HPTS) and in the root elongation zone (R-GECO1),
1035 as indicated with boxes.

A**B****D****C**

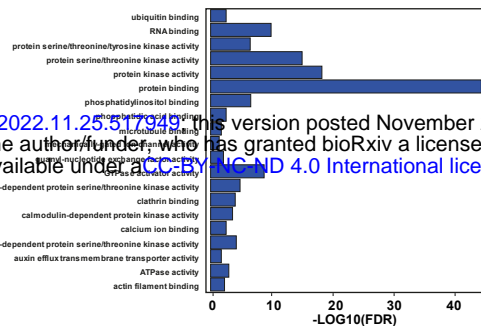




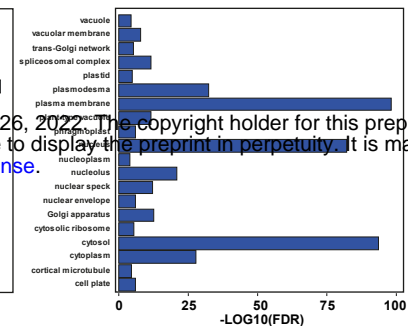
Biological process



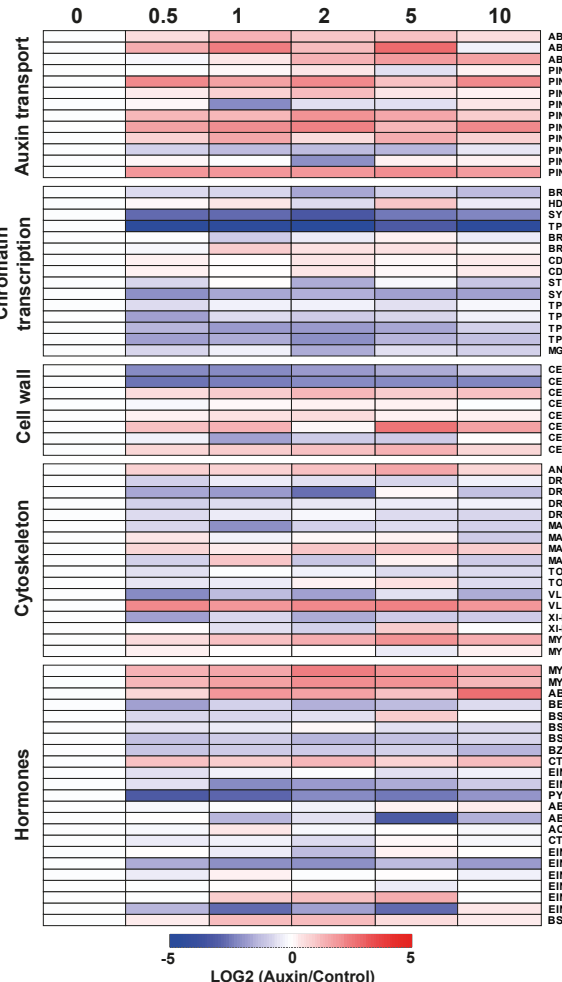
Molecular function



Cellular component



B



C

Phosphoproteome data

Phosphoproteome data									
<input type="checkbox"/> Deselect all <input type="checkbox"/> Copy <input type="checkbox"/> CSV <input type="checkbox"/> Excel <input type="checkbox"/> Show 10 <input type="checkbox"/> entries <input type="text"/> Search:									
Gene ID	Dataset	UniqueID	T0 min	T0.5 min	T1 min	T2 min	T5 min	T10 min	FDR
ABCB19_624									
ABCB19_628									
ABCB19_647									
PIN2_218									
PIN2_233									
PIN2_339									
PIN2_458									
PIN2_179									
PIN2_183									
PIN2_427									
PIN2_353									
PIN2_337									
PIN2_389									
BRM_2030									
HDAs_396									
SYD_3128									
TPL_214									
BRM_1715									
BRM_107									
CDK2_2328									
CDK2_2333									
ST1-like_3_996									
SYD_2528									
TPR_214									
TPR_2424									
TPR_2709									
TPR_314									
MGP_60									
CESA3_130									
CESA3_139									
CESA3_151									
CESA3_111									
CESA3_216									
CESA3_227									
CESA3_3									
CESA4_93									
AN_398									
DRP2A_706									
DRP2A_806									
DRP2A_877									
DRP2A_919									
MAP65_2_503									
MAP65_2_532									
MAP65_2_552									
MAP65_2_566									
TOR1_501									
TOR1_579									
VLN2_846									
VLN2_858									
XIE_1009									
XIE_141									
MYOB1_206									
MYOB1_334									
MYC2_417									
MYC2_420									
ABF4_155									
BES1_245									
BES1_245									
BSK2_25									
BSL2_891									
BZR1_224									
CTR1_710									
EIN2_645									
EIN2_524									
EIN2_524									
CTR1_155									
EIN2_599									
EIN2_1283									
EIN2_655									
EIN2_659									
EIN2_731									
EIN2_802									
BSL2_642									

Showing 1 to 10 of 28 entries (filtered from 27,914 total entries) 6 rows selected

